J|A|C|S ARTICLES

Published on Web 09/07/2010

Transmembrane Structures for Alzheimer's Aβ_{1-42} Oligomers

Birgit Strodel,*,† Jason W. L. Lee,‡ Christopher S. Whittleston,‡ and David J. Wales‡

Institut für Strukturbiologie und Biophysik, Strukturbiochemie (ISB-3), Forschungszentrum Jülich, 52425 Jülich, Germany, and University Chemical Laboratories, Lensfield Road, Cambridge CB2 1EW, United Kingdom

Received May 1, 2010; E-mail: b.strodel@fz-juelich.de

Abstract: We model oligomers of the Alzheimer's amyloid β-peptide Aβ_{1-42} in an implicit membrane to obtain insight into the mechanism of amyloid toxicity. It has been suggested that Aβ oligomers are the toxic species, causing membrane disruption in neuronal cells due to pore formation. We use basin-hopping global optimization to identify the most stable structures for the Aβ_{1-42} peptide monomer and small oligomers up to the octamer inserted into a lipid bilayer. To improve the efficacy of the basin-hopping approach, we introduce a basin-hopping parallel tempering scheme and an oligomer generation procedure. The most stable membrane-spanning structure for the monomer is identified as a β-sheet, which exhibits the typical strand-turn-strand motif observed in NMR experiments. We find ordered β-sheets for the dimer to the hexamer, whereas for the octamer, we observe that the ordered structures separate into distinct tetrameric units that are rotated or shifted with respect to each other. This effect leads to an increase in favorable peptide−peptide interactions, thereby stabilizing the membrane-inserted octamer. On the basis of these results, we suggest that Aβ pores may consist of tetrameric and hexameric β-sheet subunits. These Aβ pore models are consistent with the results of biophysical and biochemical experiments.

1. Introduction

The primary element in the pathogenesis of Alzheimer's disease (AD) is the deposition of insoluble fibril plaques in the extracellular space of the brain tissue. The major component of these plaques is the amyloid β peptide (Aβ), which is between 39 and 42 residues long and whose predominant secondary structure in the fibril is a β-sheet. Although these insoluble amyloid plaques are considered a hallmark of AD, they are not specific to AD[1] and have been observed in older patients free from AD symptoms.[2] Furthermore, it has been found that the correlations between soluble Aβ levels and severity of dementia are higher than for the amyloid plaque density.[3] This finding, together with evidence from other studies,[4,5] has led to the suggestion that oligomers, rather than the fully formed fibrils, are the toxic species.[3,6,7] It is now thought that the cytotoxicity in AD is due to membrane disruption caused by amyloid precursors, and is mediated by pore formation as the key event. Subsequent nonspecific membrane leakage[8,9] or, more likely, specific ionic transport through ion channels[10−21] could destabilize ionic homeostasis. Indeed, amyloid peptides induce ionic conductance in both artificial membranes and native cell plasma membranes,[10,14,17,19−21] and it has been found that the cytotoxicity of Aβ peptides involves the disturbance of cytosolic Ca^{2+} ion homeostasis.[22,23] Furthermore, it has been shown that

† Forschungszentrum Jülich.
‡ University Chemical Laboratories.

(1) Dickson, T. C.; Vickers, J. C. *Neuroscience* **2001**, *105*, 99–107.
(2) Jarrett, J. T.; Berger, E. P.; Lansbury Jr., P. T. *Biochemistry* **1993**, *32*, 4693–4697.
(3) Walsh, D. M.; Klyubin, I.; Fadeeva, J. V.; Cullen, W. K.; Anwyl, R.; Wolfe, M. S.; Rowan, M. J.; Selkoe, D. J. *Nature* **2002**, *416*, 535–539.
(4) Lambert, M. P.; Barlow, A. K.; Chromy, B. A.; Edwards, C.; Freed, R.; Liosatos, M.; Morgan, T. E.; Rozovsky, I.; Trommer, B.; Viola, K. L.; Wals, P.; Zhang, C.; Finch, C. E.; Krafft, G. A.; Klein, W. L. *Proc. Natl. Acad. Sci. U.S.A.* **1998**, *95*, 6448–6453.
(5) Hartley, D. M.; Walsh, D. M.; Ye, C. P.; Diehl, T.; Vasquez, S.; Vassilev, P. M.; Teplow, D. B.; Selkoe, D. J. *J. Neurosci.* **1999**, *19*, 8876–8884.
(6) Kirkitadze, M.; Bitan, G.; Teplow, D. *J. Neurosci. Res.* **2002**, *69*, 567–577.
(7) Bucciantini, M.; Giannoni, E.; Chiti, F.; Baroni, F.; Formigli, L.; Zurdo, J.; Taddei, N.; Ramponi, G.; Dobson, C. M.; Stefani, M. *Nature* **2002**, *416*, 507–511.
(8) Kayed, R.; Sokolov, Y.; Edmonds, B.; McIntire, T. M.; Milton, S. C.; Hall, J. E.; Glabe, C. G. *J. Biol. Chem.* **2004**, *279*, 46363–46366.
(9) Green, J. D.; Kreplak, L.; Goldsbury, C.; Blatter, X. L.; Stolz, M.; Cooper, G. S.; Seelig, A.; Kist-Ler, J.; Aebi, U. *J. Mol. Biol.* **2004**, *342*, 877–887.
(10) Lin, H.; Zhu, Y. W. J.; Lal, R. *Biochemistry* **1999**, *38*, 11189–11196.
(11) Lin, H.; Bhatia, R.; Lal, R. *FASEB J.* **2001**, *15*, 2433–2444.
(12) Lashuel, H.; Hartley, D.; Petre, B.; Walz, T.; Lansbury Jr., P. *Nature* **2002**, *418*, 291.
(13) Lashuel, H.; Hartley, D.; Petre, B.; Wall, J.; Simon, M.; Walz, T.; Lansbury Jr., P. *J. Mol. Biol.* **2003**, *332*, 795–808.
(14) Quist, A.; Doudevski, I.; Lin, H.; Azimova, R.; Ng, D.; Frangione, B.; Kagan, B.; Ghiso, J.; Lal, R. *Proc. Natl. Acad. Sci. U.S.A.* **2005**, *102*, 10427–10432.
(15) Arispe, N.; Rojas, E.; Pollard, H. *Proc. Natl. Acad. Sci. U.S.A.* **1993**, *90*, 567–571.
(16) Arispe, N.; Pollard, H.; Rojas, E. *Proc. Natl. Acad. Sci. U.S.A.* **1993**, *90*, 10573–10577.
(17) Arispe, N.; Pollard, H.; Rojas, E. *Mol. Cell. Biochem.* **1994**, *140*, 119–125.
(18) Arispe, N.; Pollard, H.; Rojas, E. *Proc. Natl. Acad. Sci. U.S.A.* **1996**, *93*, 1710–1715.
(19) Rhee, S. K.; Quist, A. P.; Lal, R. *J. Biol. Chem.* **1998**, *273*, 13379–13382.
(20) Kawahara, M.; Kuroda, Y.; Arispe, N.; Rojas, E. *J. Biol. Chem.* **2000**, *175*, 14077–14083.
(21) Hirakura, Y.; Carreras, I.; Sipe, J. D.; Kagan, B. L. *Amyloid* **2002**, *9*, 13–23.
(22) Mattson, M. P.; Cheng, B.; Davis, D.; Bryant, K.; Lieberburg, I.; Rydel, R. *J. Neurosci.* **1992**, *12*, 376–389.

10.1021/ja103725c

the calcium current due to Aβ insertion into lipid bilayers can be blocked,[15,18] suggesting that the calcium current is really due to channel formation, not just bilayer permeabilization by the peptide.

Atomic force microscopy (AFM) of Aβ inserted in lipid bilayers reveals ion channel-like structures, with a central pore surrounded by a wall made of oligomeric subunits.[11−14,24] Two arrangements have been identified: a rectangular structure with four apparent subunits, and hexagonal structures with six subunits. The central and outer pore diameters are about 2 and 8−12 nm, respectively.[14] From biochemical analysis, it was found that Aβ is predominantly tetrameric and hexameric in the membrane.[11] Early theoretical modeling[25] for the secondary structure of membrane-inserted $A\beta_{1-40}$ predicted an amphipathic β-hairpin for the N-terminal region spanning residues 1 to 14, followed by a short helical region with a positively charged residue (K16) at the N-terminal side and two negatively charged residues (E22 and D23) at the C-terminal side, and a second more hydrophobic helix ranging from residue N27 to V40 for the C-terminal region of $A\beta_{1-40}$.

Various experimental studies investigating the interactions between Aβ and phospholipids have revealed that Aβ prefers to bind to negatively charged lipids compared to zwitterionic lipids.[26−28] The attraction of Aβ to negatively charged lipids is dominated by electrostatic interactions,[27−29] with the phosphate on the lipid headgroup essential for Aβ binding.[30] Insertion into the membrane, however, is induced by the stabilization of the hydrophobic tail of Aβ. It was shown that Aβ can interact with cationic lipids as strongly as with anionic lipids,[27,31] and that it spontaneously inserts into lipid monolayers composed of either cationic or anionic lipids at bilayer-equivalent lipid densities and surface pressures.[27] It was further suggested that the oligomeric form of Aβ inserts to a greater extent into lipid films compared to the monomer.[27]

The effects of a membrane or a membrane-mimicking (lower dielectric constant) solvent environment on the Aβ peptide are significant and are sensitive to various physicochemical conditions, such as the concentration of the apolar medium in the solution, the charge and composition of the lipid bilayer, the ionic strength of the solution, and the pH. In numerous studies, it has been found that vesicles composed of neutral lipids do not alter the random coil solution structure of Aβ when mixed,[26,32,33] while anionic vesicles cause conversion to a β-sheet dominated structure,[26,32−35] which can be transformed to an α-helix upon further addition of anionic vesicles.[26,35] The α-helical state of Aβ has been characterized using NMR for membrane-mimicking solvent environments, including trifluoroethanol/water,[36] SDS micelles,[37−40] and hexafluoroisopropanol/water.[41,42] It was found that under these conditions Aβ consists of two helical segments, involving residues around 15−24 (helix A), around 28−36 (helix B), and a kink or turn region at residues 25−27. The kink/turn region is flexible, allowing the two helical segments to vary their relative orientation. The helical Aβ peptide resides predominantly on the micelle/membrane surface, rather than being embedded in the hydrophobic interior.[38] Only the C-terminal helix B is partially inserted into the micelle.[39,40,43] In ref 40, it was found that after the addition of zwitterionic surfactants to the SDS micelles the kink region lost its flexibility. The tightening of this segment favors intramolecular contacts between the neighboring two regions, which are no longer helical under these conditions. This transition could lead to the U-shaped strand-turn-strand motif as seen in Aβ fibrils,[44,45] followed by aggregation to β-sheet-rich structures, as observed for low SDS concentrations (below the critical micellar concentration)[35] and for anionic lipid membranes.[26,28,30,33,46−48] The authors of ref 33 concluded that the interactions between lipids and the Aβ peptide in its β-conformation may take on two different forms: a β structure that penetrates the membrane, and a β structure that is stabilized by surface binding to phospholipid headgroups. These two phenomena are not mutually exclusive and have been demonstrated to coexist for mellitin[49] and defensin[50] depending on peptide concentration and lipid characteristics.

This short summary of experimental results clearly indicates how complex the Aβ behavior in a membrane environment may be. Various computational studies on Aβ interacting with lipids have been performed to provide structural information at an atomistic level. Aβ is a cleavage product of the amyloid precursor protein (APP), which is a type-I transmembrane

(23) Mattson, M. P.; Furukawa, K. In *Alzheimer's Disease and Related Disorders: Research Advances*; Ana Asian International Academy of Aging: Bucharest, Romania, 2003.
(24) Lal, R.; Lin, H.; Quist, A. *Biochimi. Biophys. Acta* **2007**, *1768*, 1966–1975.
(25) Durell, S.; Guy, H.; Arsipe, N.; Rojas, E.; Pollard, H. *Biophys. J.* **1994**, *67*, 2137–2145.
(26) Terzi, E.; Hölzemann, G.; Seelig, J. *Biochemistry* **1997**, *36*, 14845–14852.
(27) Ege, C.; Lee, K. *Biophys. J.* **2004**, *87*, 1732–1740.
(28) Terzi, E.; Hölzemann, G.; Seelig, J. *Biochemistry* **1994**, *33*, 7434–7441.
(29) Zhao, H.; Tuominen, E.; Kinnunen, P. *Biochemistry* **2004**, *43*, 10302–10307.
(30) Chauhan, A.; Ray, I.; Chauhan, V. *Neurochem. Res.* **2000**, *25*, 423–429.
(31) Kremer, J.; Sklansky, D. J.; Murphy, R. *Biochemistry* **2001**, *40*, 8563–8571.
(32) Terzi, E.; Hölzemann, G.; Seelig, J. *J. Mol. Biol.* **1995**, *252*, 633–642.
(33) McLaurin, J.; Chakrabartty, A. *Eur. J. Biochem.* **1997**, *245*, 355–363.
(34) Meier, M.; Seelig, J. *J. Mol. Biol.* **2007**, *369*, 277–289.
(35) Wahlström, A.; Hugonin, L.; Perálvarez-Marín, A.; Jarvet, J.; Gräslund, A. *FEBS J.* **2008**, *275*, 5117–5128.
(36) Sticht, H.; Bayer, P.; Willbold, D.; Dames, S.; Hilbich, C.; Beyreuther, K.; Frank, R. W.; Rösch, P. *Eur. J. Biochem.* **1995**, *233*, 293–298.
(37) Coles, M.; Bicknell, W.; Watson, A. A.; Fairlie, D. P.; Craik, D. J. *Biochemistry* **1998**, *37*, 11064–11077.
(38) Shao, H.; Jao, S.; Ma, K.; Zagorski, M. G. *J. Mol. Biol.* **1999**, *285*, 755–773.
(39) Jarvet, J.; Danielsson, J.; Damberg, P.; Oleszczuk, M.; Gräslund, A. *J. Biomol. NMR* **2007**, *39*, 63–72.
(40) Grimaldi, M.; Scrima, M.; Esposito, C.; Vitiello, G.; Ramunno, A.; Limongelli, V.; D'Errico, G.; Novellino, E.; D'Ursi, A. M. *Biochim. Biophys. Acta, Biomembr.* **2010**, *1798*, 660–671.
(41) Crescenzi, O.; Tomaselli, S.; Guerrini, R.; Salvadori, S.; D'Ursi, A. M.; Temussi, P. A.; Picone, D. *Eur. J. Biochem.* **2002**, *269*, 5642–5648.
(42) Tomaselli, S.; Esposito, V.; Vangone, P.; van Nuland, N.; Bonvin, A.; Guerrini, R.; Tancredi, T.; Temussi, P.; Picone, D. *ChemBioChem* **2006**, *7*, 257–267.
(43) Kohno, T.; Kobayashi, K.; Maeda, T.; Sato, K.; Takashima, A. *Biochemistry* **1996**, *35*, 16094–16104.
(44) Lührs, T.; Ritter, C.; Adrian, M.; Riek-Loher, D.; Bohrmann, B.; Döbeli, H.; Schubert, D.; Riek, R. *Proc. Natl. Acad. Sci. U.S.A.* **2005**, *102*, 17342–17347.
(45) Petkova, A. T.; Yau, W. M.; Tycko, R. *Biochemistry* **2006**, *45*, 498–512.
(46) Ji, S. R.; Wu, Y.; Sui, S. F. *Gen. Physiol. Biophys.* **2002**, *21*, 415–427.
(47) Ege, C.; Majewski, J.; Wu, G.; Kjaer, K.; Lee, K. *Chem. Phys. Chem.* **2005**, *6*, 226–229.
(48) Chi, E. Y.; Ege, C.; Winans, A.; Majewski, J.; Wu, G.; Kjaer, K.; Lee, K. Y. C. *Proteins: Struct., Funct., Bioinf.* **2008**, *72*, 1–24.
(49) Monette, M.; Lafleur, M. *Biophys. J.* **1995**, *68*, 187–195.
(50) White, S. H.; Wimley, W. C.; Selsted, M. E. *Curr. Opin. Struct. Biol.* **1995**, *5*, 521–527.

glycoprotein in neural and non-neural cells, and a molecular dynamics (MD) study investigated what happens to Aβ at the moment when it is detached from APP.[51] It was found that within 100 ns the α-helical Aβ_{1-40} leaves the dipalmitoyl phosphatidylcholine (DPPC) bilayer and moves to the interface between the DPPC lipids and water, where it starts to adopt coil and bend structures. Similar results were obtained in MD studies by Lemkul and Bevan.[52,53] In a recent replica exchange molecular dynamics (REMD) study of Aβ_{1-40} and Aβ_{1-42} in a membrane environment, it was also found that the helical structures embedded in the membrane leave the hydrophobic core region and move to the membrane−solvent interface.[54] There, Aβ adopts the helix-kink-helix structure with the C-terminal helix partially inserted into the membrane, as observed in experiment.[36−42] Davis and Berkowitz followed a different approach and found that Aβ_{1-42} is attracted by both a zwitterionic DPPC and an anionic dioleoylphosphatidyserine (DOPS) lipid bilayer when it is placed above the membranes.[55] Independent of the starting structure, which was either helical or a β-hairpin, Aβ_{1-42} unfolded into structures dominated by a random coil and turns when adsorbed by the DPPC lipid bilayer, whereas at the DOPS membrane, the helicity of the helical starting structure was strongly enhanced and the β-configuration was mostly retained for the β-hairpin starting structure. These observations agree reasonably well with previous experimental results,[26,32−34] and it was concluded that the coil-to-β conversion on anionic lipid surfaces is mainly a result of protein−protein interactions between Aβ peptides.[56]

Nussinov and co-workers have performed MD simulations of Aβ in lipid bilayers.[57,58] The simulations focused on Aβ_{17-42} protofibrils, which were constructed from pentamer NMR coordinates (PDB 2BEG)[44] and exhibit the U-shaped strand-turn-strand motif. Various channel topologies containing 24 Aβ_{17-42} peptides were built, which were simulated in atomistic detail in a fully solvated 1,2-dioleoyl-*sn*-glycero-3-phosphocholine (DOPC) bilayer. During the simulations, the channels separated into ordered subunits, and the channel structures after 30 ns of MD simulation agreed with AFM images[11,14] in terms of their dimensions and shapes. The channel models were further compared with the antimicrobial peptide protegrin-1, which is a β-hairpin peptide that also forms channels in the membrane, leading to cytotoxicity and leaking of chloride ions,[59] and with functional gated channels (e.g., Na^+, K^+, and Ca^{2+}), that contain mostly α-helices and have been optimized by evolution.[60] Similar MD simulations were performed for Aβ_{9-42} and the F19P mutant of the Aβ_{17-42} peptide in another recent study.[61] As before, ion channels with loosely attached subunits were obtained, suggesting that small oligomers insert into the membrane, followed by dynamic channel assembly and dissociation. The results of this simulation study were compared to AFM images, channel conductance measurements, calcium imaging, neuritic degeneration, and cell death assays, revealing that nonamyloidogenic peptides can exert toxicity via an ion channel mechanism.[61]

The aim of the current study is to predict the structures of Aβ oligomers in a lipid bilayer. We focus on the full-length Aβ_{1-42} peptide and use basin-hopping (BH)[62,63] global optimization to identify the most stable structures for the peptide monomer and small oligomers up to the octamer. We introduce a basin-hopping parallel tempering scheme and an oligomer generation procedure to improve the performance of the BH approach in locating the global potential energy minimum for oligomers. To represent the effects of the solvent and the membrane, we use the implicit membrane model IMM1,[64] which was recently employed to study the transmembrane structures of APP.[65] From our global optimization approach, we find a membrane-spanning structure, which is inserted into the hydrophobic membrane core from residue 17 onward, and exhibits the typical strand-turn-strand motif between residues 17 and 36,[44,45] with a similar motif between residues 35 and 42. On the basis of this structure, we have identified the most stable membrane-inserted oligomers, again using BH global optimization. The resulting structures are discussed in terms of their stability and as possible candidates for the Aβ channels seen in AFM imaging.[11,14]

2. Methods

The Aβ_{1-42} peptide was represented by the united-atom force field CHARMM19.[66] The effects of the aqueous solvent and the membrane on Aβ_{1-42} were included using the IMM1 implicit membrane model,[64] which is an extension of the EEF1 implicit solvent model.[67] For the parameters of the IMM1 model, we have chosen the standard settings[64] with a width of 26 Å for the interior region of the lipid bilayer, which approximately matches the thickness of the apolar region for a DOPC bilayer. The membrane model is such that the lipid bilayer lies in the *xy*-plane and is centered at the origin of the coordinate system. We have modeled a neutral membrane since we have not employed the Gouy−Chapman term of the IMM1 model.[68] To minimize the effect of the charge state of the termini, we have acetylated the N-terminus and capped the C-terminus with the *N*-methylamide blocking group. The physiological pH of 7.4 is slightly above the pK_a of histidine (around 6.5−7.0). We have therefore chosen to model the histidines as uncharged with the proton in the δ-position, resulting in a total charge for Aβ_{1-42} of −3. However, since we use CHARMM19 together with the EFF1 solvent model, the overall peptide charge in our simulation is zero, since ordinarily charged protein groups (ionic side chains and termini) are neutralized in this model to account for the screening of the interactions between charges due to the solvent.

(51) Xu, Y.; Shen, J.; Luo, X.; Zhu, W.; Chen, K.; Ma, J.; Jiang, H. *Proc. Natl. Acad. Sci. U.S.A.* **2005**, *102*, 5403–5407.
(52) Lemkul, J. A.; Bevan, D. R. *Arch. Biochem. Biophys.* **2008**, *470*, 54–63.
(53) Lemkul, J. A.; Bevan, D. R. *FEBS J.* **2009**, *276*, 3060–3075.
(54) Miyashita, N.; Straub, J. E.; Thirumalai, D. *J. Am. Chem. Soc.* **2009**, *131*, 17843–17852.
(55) Davis, C. H.; Berkowitz, M. L. *Biophys. J.* **2009**, *96*, 785–797.
(56) Davis, C. H.; Berkowitz, M. L. *J. Phys. Chem. B* **2009**, *113*, 14480–14486.
(57) Jang, H.; Zheng, J.; Nussinov, R. *Biophys. J.* **2007**, *93*, 1938–1949.
(58) Jang, H.; Zheng, J.; Lal, R.; Nussinov, R. *Trends Biochem. Sci.* **2008**, *33*, 91–100.
(59) Jang, H.; Ma, B.; Lal, R.; Nussinov, R. *Biophys. J.* **2008**, *95*, 4631–4642.
(60) Jang, H.; Arce, F. T.; Capone, R.; Ramachandran, S.; Lal, R.; Nussinov, R. *Biophys. J.* **2009**, *97*, 3029–3037.
(61) Jang, H.; Arce, F. T.; Ramachandran, S.; Capone, R.; Azimova, R.; Kagan, B. L.; Nussinov, R.; Lal, R. *Proc. Natl. Acad. Sci. U.S.A.* **2010**, *107*, 6538–6543.
(62) Wales, D. J.; Doye, J. P. K. *J. Phys. Chem. A* **1997**, *101*, 5111–5116.
(63) Wales, D. J.; Scheraga, H. A. *Science* **1999**, *285*, 1368–1372.
(64) Lazaridis, T. *Proteins: Struct., Funct., Genet.* **2003**, *52*, 176–192.
(65) Miyashita, N.; Straub, J. E.; Thirumalai, D.; Sugita, Y. *J. Am. Chem. Soc.* **2009**, *131*, 3438–3439.
(66) Neria, E.; Fischer, S.; Karplus, M. *J. Chem. Phys.* **1996**, *105*, 1902–1921.
(67) Lazaridis, T.; Karplus, M. *Proteins: Struct., Funct., Genet.* **1999**, *35*, 133–152.
(68) Lazaridis, T. *Proteins: Struct., Funct., Bioinf.* **2005**, *58*, 518–527.

2.1. Basin-Hopping. In the basin-hopping (BH) approach to global optimization,[62,63,69] moves are proposed by perturbing the current geometry, and are accepted or rejected based upon the energy difference between the local minimum obtained by minimization from the instantaneous configuration and the previous minimum in the chain. In effect, the potential energy surface is transformed into the basins of attraction[70,71] of all the local minima, so that the energy for configuration **r** is

$$\tilde{E}(\mathbf{r}) = \min\{E(\mathbf{r})\} \quad (1)$$

where min denotes minimization. Large steps can be taken to sample this transformed landscape, since the objective is to step between local minima. Furthermore, there is no need to maintain detailed balance when taking steps, because the BH approach attempts to locate the global potential energy minimum and is not intended to sample thermodynamic properties.

To perturb the current geometry, we have the option of taking steps in dihedral angle space for the backbones and side chains of the peptides,[72] along with rigid body rotation and translation for peptide oligomers.[73] For the moves in the dihedral angle space, a certain number of the Ramachandran angles and twistable side chain dihedrals are selected and then twisted up to a maximum angle, which can be initially set by the user and is normally in the range of 20−50°. We consider dihedral angles defining planar structures, such as rings, as nontwistable in order to maintain the planar geometry.[74] To select the dihedrals, we followed earlier work and chose different twisting probabilities depending on the position along the peptide chain.[72] The relative probabilities were highest for the two ends of the chain, lowest for the middle, and varied linearly in between. The probabilities for the ends and the middle of the chain were set to 0.4 and 0.2 for the BH runs where backbone and side chain dihedrals were perturbed. In the BH runs where we only perturbed the side chain dihedrals, the probabilities were all set to 0.2.

In previous studies of peptide oligomers, we found that the combination of dihedral angle moves and rigid body motion often yields low-energy structures different from the global minimum. It proved to be difficult to find the global minimum from such geometries, since structures generated from them are generally higher in energy and tend to be rejected, so that the BH run in question becomes trapped. In the present work, we introduce two solutions to this problem. The first approach is basin-hopping parallel tempering[75−78] (BHPT) where multiple BH runs of the same system (replicas) are run simultaneously at different temperatures. A similar approach is employed in the multicanonical basin-hopping method.[79] After each BH step, replicas at neighboring temperatures can be exchanged, provided that a Metropolis criterion is satisfied for the energies of the corresponding local minima. This procedure allows high-energy structures to be accepted for the replicas at higher temperature. The associated configurational changes then migrate to the replicas at lower temperatures when exchanged with each other.

The other approach is based on generating random oligomer structures at the beginning of each BH run. In our implementation, an oligomer can be generated from monomers and other oligomers, for example, a dimer from two monomers, a trimer from a dimer plus a monomer or from three monomers, and so on. The user determines which parts of the input structure are fixed and which parts should be relocated initially. For each relocatable unit, one has to specify a minimum and maximum distance, d_{min} and d_{max}, and a minimum and maximum angle, ϕ_{min} and ϕ_{max}. The distances d_{min} and d_{max} are defined with respect to the center of mass (COM) of the fixed part of the input structure, while ϕ_{min} and ϕ_{max} are angles in the *xy*-plane of the COM. The COM of the relocatable unit in question is then moved to $d = d_{min} + r_1(d_{max} - d_{min})$ and $\phi = \phi_{min} + r_2(\phi_{max} - \phi_{min})$, where r_1 and r_2 are random numbers between zero and one. If $\phi \in [\phi_{min} = 0, \phi_{max} = 2\pi)$, the mobile unit can be placed anywhere in the *xy*-plane. If there is more than one mobile unit, it is advisable to choose ϕ_{min} and ϕ_{max} for each unit such that there is no overlap between them after relocation. The choice of d_{min} and d_{max} depends on the system. We wish to avoid atom clashes, which are governed by d_{min}, but require that the fixed and relocated units can still interact with each other, which is controlled by d_{max}. In addition to the translation, we allow the fixed and mobile units to be randomly rotated around their local COMs, with the possibility of restricting this rotation around the *z*-axis. With this approach, one is able to generate oligomers growing in the *xy*-plane. We do not apply any restrictions regarding the conformations of the individual molecules, which can be peptides, proteins, or any other component. Furthermore, the individual units can be of different types and can be proteins or nonproteinaceous molecules. If one considers a dimer and allows rigid body rotation for both units in the full space, one can generate, in principle, all possible dimer configurations. This approach is thus suitable for probing the binding modes of protein−protein and protein−ligand complexes.

After their initial generation, the oligomers are optimized using BH with dihedral angle moves and small rigid body rotations and translations applied to the individual peptides. We have tested this approach for the KFFE dimer and find it to be much more successful in identifying the global minimum than our previous scheme.[73] For instance, if we generate 100 random dimer structures and optimize each for 100 BH steps, which can be done in parallel, we always find the global minimum. However, if we instead generate one random dimer and optimize it for 10 000 BH steps, the global minimum can be missed. In the current work, we employ our BHPT approach with initial oligomer generation to investigate $A\beta_{1-42}$ dimers to octamers in the membrane. If not otherwise stated, the temperature was set to 300 K in the BH runs. In the BHPT runs, the exchange probability was set to 0.5. Sample input for such a BH run together with annotations is provided as Supporting Information.

The BH algorithm, including BHPT and the oligomer generation procedure, has been implemented in the GMIN program.[80] Although the BHPT approach was introduced some time ago, we have not described it before because standard BH runs have usually proved to be sufficient for clusters composed of atoms or small molecules. Basin-hopping has already been employed to find the global minimum of peptides and proteins in previous work.[72,81−86] Similar global optimization approaches have also been applied to biomolecules, including a modified BH technique combined with evolu-

(69) Li, Z.; Scheraga, H. A. *Proc. Natl. Acad. Sci. U.S.A.* **1987**, *84*, 6611–6615.
(70) Mezey, P. G. *Potential Energy Hypersurfaces*; Elsevier: Amsterdam, 1987.
(71) Wales, D. J. *J. Chem. Soc., Faraday Trans.* **1992**, *88*, 653–657.
(72) Mortenson, P. N.; Wales, D. J. *J. Chem. Phys.* **2001**, *114*, 6443–6454.
(73) Strodel, B.; Wales, D. J. *J. Chem. Theory Comput.* **2008**, *4*, 657–672.
(74) Bauer, M.; Strodel, B.; Fejer, S.; Koslover, E.; Wales, D. *J. Chem. Phys.* **2010**, *132*, 054101.
(75) Swendsen, R. H.; Wang, J.-S. *Phys. Rev. Lett.* **1986**, *57*, 2607–2609.
(76) Geyer, G. In *Computing Science and Statistics: Proceedings of the 23rd Symposium on the Interface*. Keramidas, E. K., Ed.; Inferface Foundation: Fairfax Station, 1991; p 156.
(77) Tesi, M. C.; van Rensburg, E. J. J.; Orlandini, E.; Whittington, S. G. *J. Stat. Phys.* **1996**, *82*, 155–181.
(78) Hukushima, K.; Nemoto, K. *J. Phys. Soc. Jpn.* **1996**, *65*, 1604–1608.
(79) Zhan, L.; Chen, J. Z. Y.; Liu, W.-K.; Lai, S. K. *J. Chem. Phys.* **2005**, *122*, 244707.
(80) Wales, D. J. GMIN: A program for basin-hopping global optimization. http://www-wales.ch.cam.ac.uk/software.html.
(81) Derreumaux, P. *J. Chem. Phys.* **1997**, *106*, 5260–5270.
(82) Derreumaux, P. *J. Chem. Phys.* **1997**, *107*, 1941–1947.
(83) Mortenson, P. N.; Evans, D. A.; Wales, D. J. *J. Chem. Phys.* **2002**, *117*, 1363–1376.
(84) Carr, J. M.; Wales, D. J. *J. Chem. Phys.* **2005**, *123*, 234901.
(85) Verma, A.; Schug, A.; Lee, K. H.; Wenzel, W. *J. Chem. Phys.* **2006**, *124*, 044515.

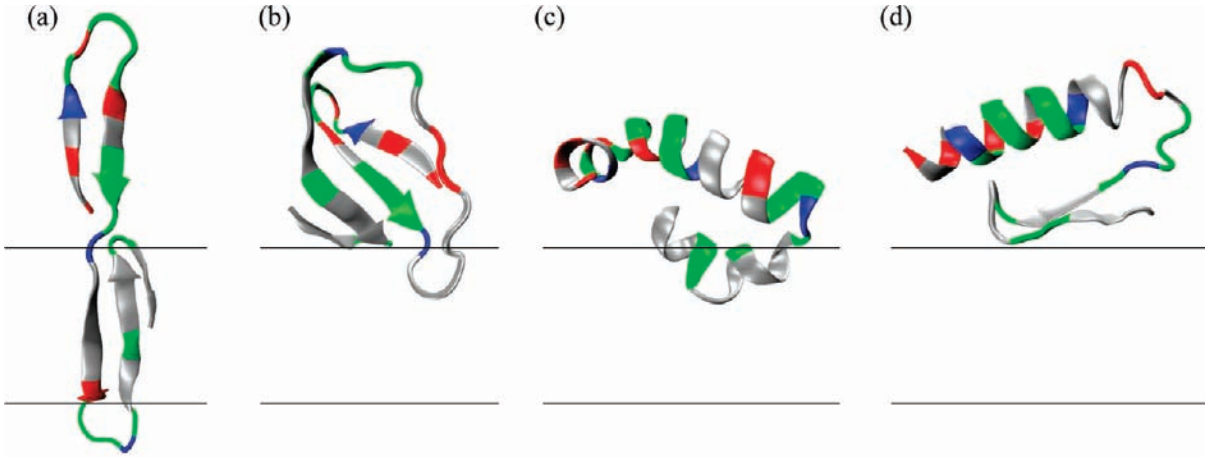

Figure 1. Low-lying structures in terms of potential energy are shown for the Aβ_{1-42} monomer: (a) the membrane-spanning β-sheet; (b) the β-sheet structure adsorbed on the surface, which was found to be lowest in energy; (c) the helix-kink-helix structure at the membrane-water interface, which was identified as the next most stable structure; and (d) a structure with a mixed helical/ β-sheet conformation. The residues are colored according to their physicochemical properties (blue, basic; red, acidic; gray, hydrophobic; green, polar); the sequence of Aβ_{1-42} is D1-A2-E3-F4-R5-H6-D7-S8-G9-Y10-E11-V12-H13-H14-Q15-K16-L17-V18-F19-F20-A21-E22-D23-V24-G25-S26-N27-K28-G29-A30-I31-I32-G33-L34-M35-V36-G37-G38-V39-V40-I41-A42. The black lines denote the boundary between the hydrophobic core and polar headgroup regions of the membrane.

tionary steps,[87−89] the activation-relaxation algorithm,[90] and basin-hopping with MD moves to generate the new conformations for minimization.[91,92] The GMIN program also allows for MD moves, here in combination with the CHARMM program,[93] instead of dihedral moves. However, our tests indicate that dihedral angle moves can be more efficient, both in terms of computing time and in locating low-energy structures. To increase the efficiency of MD moves, one could modify the dynamics by sampling only the slow vibrational modes.[92] An alternative is to use alternating random dihedral moves and MD. Our tests indicate that the MD makes this approach computationally more expensive than random moves only, but low-energy structures may be located in fewer BH steps. In a future study, we will provide a more detailed comparison of these various BH schemes. However, for oligomers, we were not able to generate oligomer structures efficiently with MD moves, and this approach was thus not considered further here.

Basin-hopping techniques have already been used to explore amyloid assembly for short peptide sequences, for instance for the KFFE peptide[79,94−97] and Aβ_{16-22}.[98,99] The current study is, to the best of our knowledge, the first one to search for the global minimum of a longer amyloidogenic peptide, such as Aβ_{1-42}, and its oligomers in a membrane environment. In a recent study, simulated annealing was employed to search for the global minimum of a peptide/bilayer system.[100] The BH global optimization approach should enable us to locate low-lying structures much faster and more reliably.

3. Results and Discussion

3.1. Monomer. 3.1.1. Results from Global Optimization. Global optimization using BH identified a membrane-spanning structure, which is shown in Figure 1a. The more hydrophobic C-terminal region starting from residue 17 is fully inserted into the apolar part of the lipid bilayer, forming an antiparallel β-sheet with two turn regions, the first ranging from residue 23 to 29 and the second one involving residues 37 and 38. The first turn is prominent in the experimentally determined structures of Aβ fibrils[44,45] and is persistent in MD simulations assessing the stability of preformed fibrillar assemblies.[101] The NMR solution structures of various Aβ fragments[102,103] and the Aβ_{1-42} dimer[104] suggest that this feature is also present in both Aβ oligomers and the monomer. A REMD study[105] of Aβ_{16-35} also found a loop at positions 22−28 in the monomer and dimer. The residues of the first turn region, which are mostly hydrophilic and charged, are in or close to the polar headgroup region of the lower bilayer leaflet. The second turn, which is hydrophilic, is in the proximity of the headgroup region of the upper layer and leads to a β-sheet involving the hydrophobic residues 39−42. The extra two hydrophobic residues I41 and A42 make the antiparallel β-sheet more stable compared to Aβ_{1-40}, which has a high propensity to bury in the hydrophobic core of the lipid bilayer,[106] perhaps explaining the greater toxicity of Aβ_{1-42}

(86) Verma, A.; Wenzel, W. *J. Phys.: Condens. Matter* **2007**, *19*, 285213.
(87) Schug, A.; Wenzel, W. *J. Am. Chem. Soc.* **2004**, *126*, 16736–16737.
(88) Schug, A.; Wenzel, W. *Biophys. J.* **2006**, *90*, 4273–4280.
(89) Verma, A.; Gopal, S. M.; Oh, J. S.; Lee, K. H.; Wenzel, W. *J. Comput. Chem.* **2007**, *28*, 2552–2558.
(90) Wei, G.; Derreumaux, P.; Mousseau, N. *J. Chem. Phys.* **2003**, *119*, 6403.
(91) Goedecker, S. *J. Chem. Phys.* **2004**, *120*, 9911–9917.
(92) Roy, S.; Goedecker, S.; Field, M. J.; Penev, E. *J. Phys. Chem. B* **2009**, *113*, 7315–7321.
(93) Brooks, B.; et al. *J. Comput. Chem.* **2009**, *30*, 1545–1614.
(94) Melquiond, A.; Boucher, G.; Mousseau, N.; Derreumaux, P. *J. Chem. Phys.* **2005**, *122*, 174904.
(95) Wei, G.; Mousseau, N.; Derreumaux, P. *J. Phys.: Condens. Matter* **2004**, *16*, 5047–5054.
(96) Wei, G.; Mousseau, N.; Derreumaux, P. *Biophys. J.* **2004**, *87*, 3648–3656.
(97) Melquiond, A.; Mousseau, N.; Derreumaux, P. *Proteins: Struct., Funct., Bioinf.* **2006**, *65*, 180–191.
(98) Santini, S.; Wei, G.; Mousseau, N.; Derreumaux, P. *Structure* **2004**, *12*, 1245–1255.
(99) Santini, S.; Mousseau, N.; Derreumaux, P. *J. Am. Chem. Soc.* **2004**, *126*, 11509–11516.
(100) Fuzo, C. A.; Castro, J. R. M.; Degréve, L. *Int. J. Quantum Chem.* **2008**, *108*, 2403–2407.
(101) Ma, B.; Nussinov, R. *Proc. Natl. Acad. Sci. U.S.A.* **2002**, *99*, 14126–14131.
(102) Lazo, N. D.; Grant, M. A.; Condron, M. C.; Rigby, A. C.; Teplow, D. B. *Protein Sci.* **2005**, *14*, 1581–1596.
(103) Lee, J. P.; Stimson, E. R.; Ghilardi, J. R.; Mantyh, P. W.; Lu, Y.-A.; Felix, A. M.; Llanos, W.; Behbin, A.; Cummings, M. *Biochemistry* **1995**, *34*, 5191–5200.
(104) Yu, L.; et al. *Biochemistry* **2009**, *48*, 1870–1877.
(105) Chebaro, Y.; Mousseau, N.; Derreumaux, P. *J. Phys. Chem. B* **2009**, *113*, 7668–7675.
(106) Mobley, D. L.; Cox, D. L.; Singh, R. R. P.; Maddox, M. W.; Longo, M. L. *Biophys. J.* **2004**, *86*, 3585–3597.

compared to Aβ1−40. The existence of the turn centered at residues 37 and 38 and its possible importance for the aggregation of Aβ1−42 have already been discussed in previous work.[107−109] In the membrane-spanning structure shown in Figure 1a, the more polar and charged N-terminal part of Aβ1−42 is in the polar headgroup region, which lies outside the implicit membrane, thus, avoiding contact with hydrophobic lipid tails. We find an amphipathic β-hairpin for this part of the peptide, as predicted by Durell et al.,[25] with the hydrophilic D1, E3, R5, D7, E11, and H13 residues on one side, the hydrophobic A2, F4, and V12 on the other side, and stabilizing salt bridges E4−R6 and E12−R6. According to Hecht and collaborators, such a pattern indicates a high β propensity.[110] However, to the best of our knowledge, a β-hairpin for the N-terminal region has so far not been observed experimentally for either the monomer, oligomers, or the fibril. Instead, in most cases, the structure for this part of Aβ cannot be resolved experimentally due to the flexibility of residues 1−16. However, in another simulation study, an N-terminal β-hairpin has also been distinguished.[109] In the current simulation, the occurrence of this β-hairpin may be due to the implicit solvent/membrane model, which omits explicit solute−solvent interactions that are probably of importance for the secondary structure of Aβ in this region. The assumption that the potential of mean force can be applied to approximate the averaged behavior of many highly dynamic solvent molecules is probably most likely to fail for this region. A future study will investigate the structural changes that the conformation in Figure 1a undergoes when it is immersed in an explicit solvated membrane.

The structure in Figure 1a was found from a completely extended conformation, with a random overall orientation and all Ramachandran angles initialized to 180°. Because of the length of the extended structure (about 150 Å), in most starting orientations, Aβ1−42 crossed both membrane surfaces. In addition to the extended structure, we have also considered a helical conformation[42] (PDB 1Z0Q) as the starting structure, which was also randomly oriented. For both initial conformations, we have performed 200 BH runs with 3000 steps each, resulting in a total of 12 000 000 BH steps. Since we wanted to focus on membrane-bound structures, we had to prevent Aβ1−42 drifting out of the membrane before it could adapt to the local environment. We therefore added repulsive walls of the form[111]

$$V_{\mathrm{rep}}(z) = \frac{4\pi eZ}{5z}\left[\left(\frac{\sigma}{z-Z}\right)^{10} - \left(\frac{\sigma}{z+Z}\right)^{10}\right] \qquad (2)$$

where the parameters σ and e were set to 1 Å and 1 kcal mol^{-1}, respectively. The constant Z denotes the location of the wall, which we chose as $Z = 40$ Å. Thus, the repulsive potential takes effect at 27 Å above and below the surface of the upper and lower membrane regions, respectively, leaving sufficient room for Aβ1−42 to reorganize at the membrane surface while preventing it from completely drifting away. For each of the 400 BH runs, we saved 10 low-energy structures separated by at least 3 kcal mol^{-1} from each other. Here, we discuss stability in terms of the potential energy, which is a sum of intramolecular and solvation terms. This quantity is sometimes referred to as an effective energy. For 12% of the BH runs, the potential energy of the lowest-energy structure was below −1245 kcal mol^{-1}. More steps would be required to reach energies below this value in the other BH runs. All of the recorded lowest-energy structures correspond to the peptide adsorbed at the membrane surface rather than embedded in the membrane. Only about 1% of all the recorded 4000 structures were transmembrane structures, of which the six lowest in energy involve the transmembrane β-sheet in Figure 1a. This geometry was thus identified as the most stable membrane-inserted structure with $E = -1226.5$ kcal mol^{-1}.

To ensure that we did not miss structures of lower energy, we performed another 48 BH runs of 3000 steps starting from the structures with energies below −1245 kcal mol^{-1}. The largest energy decrease was less than 1 kcal mol^{-1}, originating from small side chain reorientations. Visual inspection of the final 48 structures revealed a high conformational diversity, including α-helical and β-sheet conformations, but also structures with a high degree of random coil. This finding is in agreement with the experimental observation that Aβ can adopt helical[26,35] and β-sheet conformations[26,32−35] or an intermediate structure between these two,[40] but can adopt random coil geometries when residing at the surfaces of neutral bilayers.[26,32,33] We thus conclude that the alternative low-lying minima for membrane-bound Aβ are probably separated by high barriers, corresponding to a rugged, frustrated energy landscape, in contrast to the minimal frustration[112,113] expected for a good structure-seeking system.[114] To further investigate this hypothesis, thermodynamic sampling is required in order to obtain information about the conformational entropies of these structures and the energetic barriers between them. We plan to address these issues in future work.

The lowest-energy structure that we identified in eight of the 400 BH runs is shown in Figure 1b with $E = -1260.2$ kcal mol^{-1}. Similar structures with Aβ1−42 halfway inserted into the membrane were observed as well, but their energies are 20−30 kcal mol^{-1} higher. Hence, the insertion of a single Aβ1−42 peptide seems to be an unlikely process, in agreement with experimental observations that low surface pressures are needed for Aβ to insert into a neutral membrane, and that Aβ oligomers insert more easily than the monomer.[27] The second lowest-energy structure, which was identified in six of the 400 BH runs, is a helical conformation shown in Figure 1c with $E = -1255.7$ kcal mol^{-1}. It has some features in common with the previously reported helix-kink-helix structures from NMR measurements[36−42] and a REMD simulation.[54] Compared to these structures, helix A is extended to include residues 8−27, followed by a short kink at positions 28 and 29 instead of 25−27. The kink leads to helix B, which is partially inserted into the membrane core, as previously observed in experiment[39,40,43] and simulation.[54] The overall minor differences between the most stable structures identified from the REMD simulation in ref 54 and the one in Figure 1c may be attributed to differences in the potentials and the different sampling methods. REMD identifies the free energy minima, while BH

(107) Urbanc, B.; Cruz, L.; Yun, S.; Buldyrev, S. V.; Bitan, G.; Teplow, D. B.; Stanley, H. E. *Proc. Natl. Acad. Sci. U.S.A.* **2004**, *101*, 17345–16350.
(108) Huet, A.; Derreumaux, P. *Biophys. J.* **2006**, *91*, 3829–3840.
(109) Melquiond, A.; Dong, X.; Mousseau, N.; Derreumaux, P. *Curr. Alzheimer Res.* **2008**, *5*, 244–250.
(110) Xiong, H.; Buckwalter, B.; Shieh, H.; Hecht, M. *Proc. Natl. Acad. Sci. U.S.A.* **1995**, *92*, 6349–6353.
(111) Klimov, D. K.; Newfield, D.; Thirumalai, D. *Proc. Natl. Acad. Sci. U.S.A.* **2002**, *99*, 8019–8024.
(112) Bryngelson, J. D.; Onuchic, J. N.; Socci, N. D.; Wolynes, P. G. *Proteins: Struct., Funct., Genet.* **1995**, *21*, 167–195.
(113) Onuchic, J. N.; Luthey-Schulten, Z.; Wolynes, P. G. *Annu. Rev. Phys. Chem.* **1997**, *48*, 545–600.
(114) Wales, D. J. *Curr. Opin. Struct. Biol.* **2010**, *20*, 3–10.

searches for the global minimum of the (effective) potential energy. We have located several local minima with the kink at residues 25−27 and similar lengths for helices A and B with energies around 5 kcal mol^{-1} above that of the structure in Figure 1c. Hence, our BH results are in overall good agreement with previous experimental[36−42] and simulation[54] data.

Another interesting structure found from the BH runs is presented in Figure 1d. It consists of a helix from residues 1 to 22, followed by a loop involving residues 23−28, and a β-hairpin formed by the remaining residues. The energy of this structure is −1249.4 kcal mol^{-1}. The existence of this state is evidence of the high propensity of the segment 30−42 to form stable hydrogen bonds, that is, to form either α-helices or β-sheets.[35] The structure in Figure 1d may also represent an intermediate conformation between membrane-bound helix-kink-helix conformations and the strand-turn-strand motif observed for Aβ aggregates.

3.1.2. Results from Thermodynamic Sampling. To further test the thermodynamic stability of the membrane-spanning β-sheet in Figure 1a, we performed a REMD simulation with 16 replicas between 270 and 500 K initiated from this structure. The simulation consisted of 100 000 replica exchange cycles with each cycle involving 500 MD steps of 2 fs, resulting in a simulation time of 100 ns for each replica, that is, a total simulation time of 1.6 μs. The dynamics were propagated using the Langevin method with a friction coefficient of $\zeta = 5$ ps^{-1}. The REMD simulation was conducted with the MMTSB tool set[115] interfaced to the CHARMM19 EEF1.1 force field,[64,116] which includes the IMM1 implicit membrane model.[64] The results show that the transmembrane β-sheet is very stable in terms of secondary structure and its position within the membrane, since the peptide does not leave the membrane or undergo any major conformational changes in any of the replicas. The free energy at $T = 300$ K projected along the root-mean-square deviation (rmsd) from the initial structure, as generated using the weighted histogram analysis method,[117] shows two free energy minima for the backbone rmsd at about 2 and 4 Å (data not shown). The latter value is due to small changes in the N-terminal β-hairpin, while the β-sheet structure in the membrane core does not change. In an MD simulation at 300 K using an explicit bilayer and a different force field, we have also observed high stability for this membrane-immersed β-sheet.[118]

We thus conclude that this is a stable transmembrane structure due to anchoring of the β-sheet in the membrane by the hydrophilic residues K16, E22−K28, and G37−G38 at the headgroup−core interfaces. These residues cause a high energetic barrier for the structure to move in either direction perpendicular to the membrane, as evidenced by the free energy profiles for small molecules mimicking natural amino acids traversing lipid bilayers.[119] This anchoring effect also restricts conformational changes for the hydrophobic residues in the membrane core. It seems that the β-sheet in Figure 1a matches the thickness of 26 Å of the membrane core, whereas helical conformations seem too short to stabilize such a transmembrane structure. As a result, helical structures immersed in a membrane often move to position themselves at the water/bilayer interface, as seen in previous MD simulations with explicit bilayers[51,52] and in experiment.[39,40,43] We note, however, that in some of the 100 ns MD runs in ref 52 the helical peptides did not leave the DPPC bilayer. Instead, the peptide adopted a transmembrane structure, either in an extended or partially helical conformation, remaining in contact with the headgroup region of the lower membrane boundary via the C-terminus. These results suggest that the transmembrane helix is not stable and would probably convert to a more extended structure if simulated for longer time scales. This conclusion is somewhat different from the results of Mobley et al.,[106] which predicted a transmembrane helix for Aβ_{1-42}. This study, however, uses a coarse-grained peptide representation in connection with an implicit membrane model, which is biased toward α-helices according to the authors.[106]

On the basis of our results, and the above considerations, we decided to use the transmembrane β-sheet identified from our BH approach as the basic unit for the generation of oligomers. Our decision is supported by the results of a recent study on the structure−neurotoxicity relationships of Aβ_{1-40} oligomers, which showed that the β-content increases with oligomer size and that tetramers are the most toxic assembly compared to monomers, dimers, trimers, and fibrils.[120] However, in the same study, and another investigation based on simulation,[109] it was suggested that the assembly in aqueous solution from the monomer to the dimer is accompanied by a significant reorganization of the Aβ peptide, which will be not captured by our approach that assumes the β-state for the individual peptides during the assembly process. The present methodology is justified because our investigation focuses on structure prediction for membrane-inserted oligomers, rather than the oligomerization pathway itself. We also note that our simulations do not address the insertion process for Aβ in the membrane. Rather, our structural survey suggests that from the enthalpic viewpoint the penetration of an individual Aβ peptide seems an unlikely event. A previous simulation study of a model hexapeptide consisting of a tryptophan and five leucines concluded that the most likely insertion/aggregation mechanism is a pathway where the peptide first adheres to the solvent−headgroup interface, aggregates, and then inserts.[121] It remains to be seen whether Aβ would follow a similar pathway.

3.2. Oligomers. For the investigation of oligomer structures in the membrane, we used the single membrane-spanning β-sheet shown in Figure 1a and generated oligomers from it as described in section 2.1. We investigated dimers, trimers, tetramers, hexamers, and octamers to identify the most stable structures as possible candidates for Aβ pores in the membrane.[11−14,24,25] The oligomers we investigated are thus limited to structures where the hydrophobic C-terminal regions of the Aβ_{1-42} peptides are fully buried in the apolar core of the membrane. Hence, we only allowed rotation around the *z*-axis and translation in the *xy*-plane for the generation of oligomers. The resulting structures were further optimized by performing between 70 and 200 BH steps with random dihedral angle moves applied to the side chains, random rigid body rotation around the *z*-axis, and translation in the *xy*-plane. For the side chain moves, we allowed dihedral angle changes of up to 20° with a

(115) Feig, M.; Karanicolas, J.; Brooks, C. L. *J. Mol. Graphics Modell.* **2004**, *22*, 377–395.
(116) Masunov, A.; Lazaridis, T. *J. Am. Chem. Soc.* **2003**, *125*, 1722–1730.
(117) Kumar, S.; Bouzida, D.; Swendsen, R. H.; Kollman, P. A.; Rosenberg, J. M. *J. Comput. Chem.* **1992**, *13*, 1011–1021.
(118) Poojari, C.; Strodel, B. Unpublished results, 2010.
(119) MacCallum, J. L.; Bennetta, W. F. D.; Tieleman, D. P. *Biophys. J.* **2008**, *94*, 3393–3404.
(120) Ono, K.; Condron, M. M.; Teplow, D. B. *Proc. Natl. Acad. Sci. U.S.A.* **2009**, *106*, 14745–14750.
(121) Babakhani, A.; Gorfe, A. A.; Kim, J. E.; McCammon, J. A. *J. Phys. Chem. B* **2008**, *112*, 10528–10534.

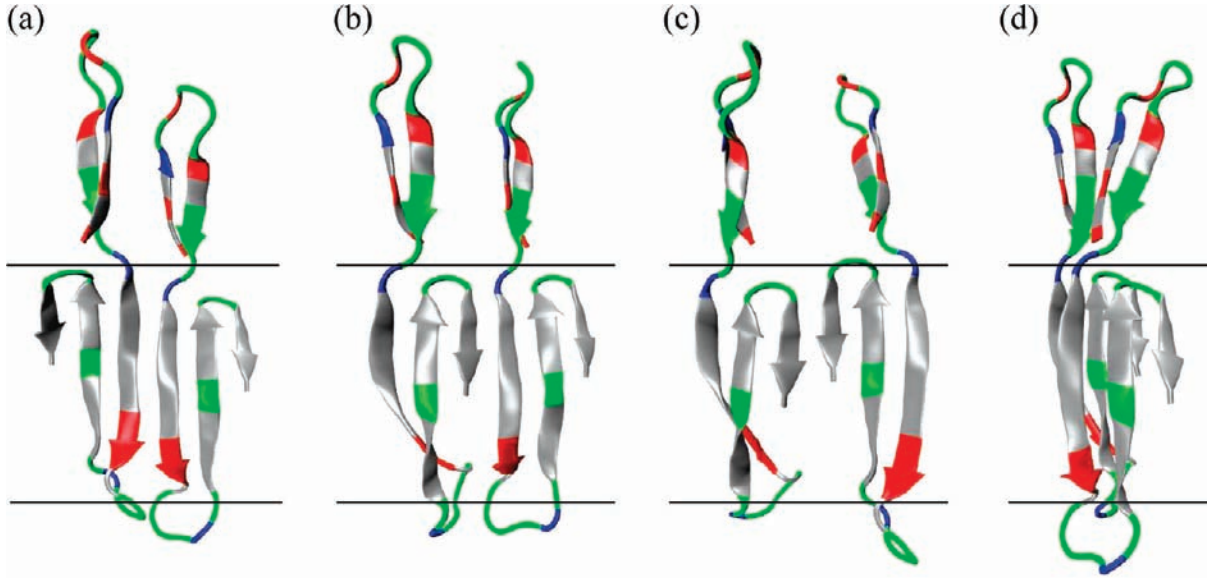

Figure 2. Dimer structures (a) CNNC, (b) NCNC, (c) NCCN, and (d) 2NCb. The residues are colored according to their physicochemical properties: blue, basic; red, acidic; gray, hydrophobic; green, polar. The black lines denote the boundary between the hydrophobic core and polar headgroup regions of the membrane.

uniform probability of 0.2. The individual peptides were rotated by an angle smaller than 90° in either direction and translated with a maximum displacement of 2 Å. The probability of rigid body motion for the individual peptide was set to $1/n$, where n refers to the size of the oligomer, that is, $n = 2$ for a dimer, $n = 3$ for a trimer, and so on. The number of structures generated depends on n and the detailed generation protocols for each oligomer are given below.

3.2.1. Dimers. We generated 100 dimers from two monomers by placing the second monomer at a distance between 9 and 18 Å from the first peptide at a random angle $\phi \in [0, 2\pi)$ in the xy-plane. Each starting point was optimized for 200 BH steps, resulting in 18 structures with a potential energy below -2500 kcal mol^{-1}. The lowest-energy minimum with $E = -2506.3$ kcal mol^{-1} is shown in Figure 2a. Inside the apolar membrane core, this structure is characterized by interactions between the hydrophobic lipid tails and the two C-terminal regions of $A\beta_{1-42}$, while the peptides interact with each other by forming a β-sheet involving residues 17−23 of each monomer. We denote this structure as CNNC since the C-termini point outward and the N-terminal regions form an interface.[59] This structure is also stabilized by van der Waals interactions between the two β-hairpins outside the hydrophobic core. However, as these β-hairpins may not be stable when modeled in an explicit bilayer environment, we do not wish to use the stabilization energies originating from outside the hydrophobic membrane core as an argument for the overall stability of the oligomer structures. On the other hand, it is probably important to model the full-length Aβ in order to identify the interactions between the polar headgroup region and Aβ and make predictions for possible Aβ membrane pore structures.

Another stable dimer structure with $E = -2502.8$ kcal mol^{-1}, denoted NCNC, is shown in Figure 2b. In this case, the peptides are arranged next to each other, so that in the hydrophobic core the C-terminal region of the first peptide forms a β-sheet with the N-terminal region of the second peptide. Although the interface between the two peptides is smaller than in the CNNC dimer, the stabilization energies due to electrostatic and van der Waals interactions between the peptides, as well as the free energies of solvation inside and outside the hydrophobic core, are very similar (cf. Table 1).

Table 1. Potential Energies, E, Peptide−Peptide Interaction Energies (Divided into Electrostatic, E_{int}^{el}, and van der Waals, E_{int}^{vdW}, Terms), and Solvation Free Energies, ΔG_{solv}, for Membrane-Inserted Dimers[a]

		outside hydrophobic core			inside hydrophobic core		
dimer	E	E_{int}^{el}	E_{int}^{vdW}	ΔG_{solv}	E_{int}^{el}	E_{int}^{vdW}	ΔG_{solv}
CNNC	−2506.3	−2.4	−36.7	−396.4	−42.8	−39.7	−195.5
NCNC	−2502.8	−4.9	−33.7	−391.2	−35.7	−44.4	−204.4
NCCN	−2476.6	−9.2	−9.9	−402.9	−18.6	−18.5	−217.8
2NCb	−2497.1	−31.2	−44.4	−384.4	−13.0	−32.6	−209.2

[a] All energies are in kcal mol^{-1} and are divided into the contributions from outside and inside the hydrophobic core of the membrane.

We also identified NCCN arrangements where the C-terminal regions form a short β-sheet, as shown in Figure 2c, leading to a reduction in interpeptide interactions. This reduction is only partially compensated by an increase in interactions between the peptides and the membrane inside and outside the hydrophobic core, resulting in an overall increase in potential energy of about 25−30 kcal mol^{-1} compared to the CNNC and NCNC dimers. Another stable dimer with $E = -2497.1$ kcal mol^{-1} has the two β-sheets behind each other, and is denoted 2NCb in Figure 2d. However, this structure is largely stabilized by interpeptide interactions outside the hydrophobic membrane core (cf. Table 1). It is thus possible that this dimer structure will not be as stable when modeled with an explicit membrane model. The CNNC, NCNC, and 2NCb arrangements, but not NCCN, dominate the stable structures for the higher oligomers discussed below.

To ensure that we have not missed any transmembrane dimer structure lower in energy than those presented in Figure 2, we have performed 400 BH runs with 3000 steps each using a template-based approach. Here, we added to the transmembrane β-sheet another $A\beta_{1-42}$ peptide in either a fully extended, helical (PDB 1Z0Q), or mainly coiled conformation. For the latter geometry, we used two different structures with varying amounts of helical and β-sheet content, as extracted from an MD simulation in explicit solvent at 300 K. The added peptide was

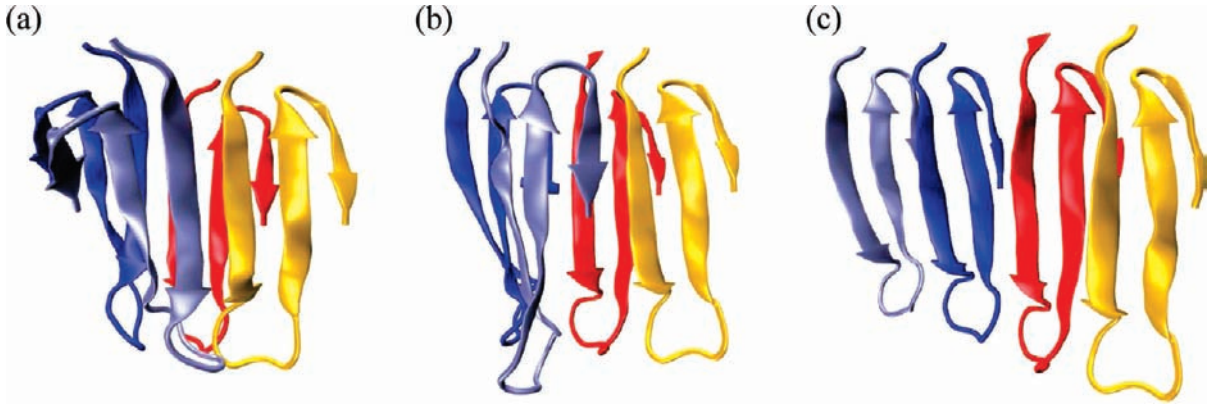

Figure 3. The hydrophobic core-spanning parts of the tetramer structures (a) 2CNNCb, (b) 2NCNCb, (c) 4NCb. For each Aβ_{1-42} peptide, only residues 17−42 are illustrated. The color scheme for the peptides was chosen for clarity.

randomly rotated in the full three-dimensional space and positioned in the *xy*-plane around the initial β-sheet at a distance between 9 and 18 Å. During the subsequent optimization, we applied random moves to the added peptide including rigid body translation in the *xy*-plane and rotation in full space as well as changes in the dihedral angles of the backbone and side chains. The transmembrane β-sheet, on the other hand, was only allowed to relax during the minimization steps. None of the resulting dimers were lower in energy than the CNNC, NCNC, and 2NCb dimers described above. Most of the lowest energy structures found using this approach consist of the transmembrane β-sheet and a membrane-adsorbed conformation similar to the conformations shown in Figure 1b−d. This result again shows the high propensity of Aβ_{1-42} to adhere to the membrane surface.

3.2.2. Trimers and Tetramers. Tetramers were either generated (i) from four monomers, (ii) from two dimers, or (iii) by adding a monomer to a trimer. In approach (i), we added three peptides to an initial monomer at a distance between $d_{min} = 9$ Å and $d_{max} = 18$ Å. To prevent atom clashes on placing two peptides too close to each other, the first added peptide was placed at an angle $\phi_1 \in [0, 2\pi/3)$, the second one at $\phi_2 \in [2\pi/3, 4\pi/3)$, and the third at $\phi_3 \in [4\pi/3, 2\pi)$. We generated 200 tetramers using this approach. For the generation of tetramers from dimers in (ii), we used the dimer structures shown in Figure 2. We always added two dimers of the same kind together. The second dimer was placed at a distance between 18 and 28 Å from the first one at a random angle in the *xy*-plane. From each dimer, 120 tetramer structures were generated, resulting in 480 tetramers. The trimer structures employed in approach (iii) were generated from three monomers in a previous simulation. From 200 of these trimers, we identified triangular structures and planar β-sheets (NCNCNC and CNNCNC) as the most stable structures. The triangular structures are approximately equilateral, with one of the edges formed by one of the stable dimer β-sheets. Four of these trimer structures, two triangular and two planar, were used to generate a total of 1120 tetramer structures. To restrict the location of the monomer added to each of the trimers, we used the values $d_{min} = 9$ Å, $d_{max} = 18$ Å and $\phi \in [0, 2\pi)$.

We thus generated 1800 tetramers in total. Each structure was optimized for 150 BH steps, corresponding to 270 000 BH steps in total. All low-energy structures have two dimers behind each other, forming a double-layered β-sheet. The two most stable arrangements are composed of two CNNC dimers ($E = -5095.9$ kcal mol^{-1}) and two NCNC dimers ($E = -5083.5$ kcal mol^{-1}), as shown in Figure 3, panels a and b, and denoted 2CNNCb and 2NCNCb, respectively. The structures with four Aβ_{1-42} peptides in a row have a substantially higher energy than the latter two arrangements. One such structure with $E = -5042.5$ kcal mol^{-1} is shown in Figure 3c and denoted 4NCb, because in the membrane the peptides are behind each other, rather than forming a β-sheet. A detailed analysis of the energies shows that tetramers 2CNNCb and 2NCNCb are largely stabilized by interpeptide interactions, which are clearly reduced in 4NCb. For the latter structure, the free energy of solvation is lower than for the former two due to its larger solvent-accessible surface area. This energy reduction is, however, not sufficient to compensate for the reduced interpeptide interactions in 4NCb.

3.2.3. Hexamers. The trend that dimers prefer to arrange behind each other rather than forming single-layered β-sheets was also observed for the most stable hexamer structures. We generated 200 hexamers for each of five different approaches: (i) six monomers ($\phi_i \in [2(i-1)\pi/5, 2i\pi/5)$ with $i = 1, ..., 5$), (ii) three CNNC dimers ($\phi_1 \in [0, \pi)$, $\phi_2 \in [\pi, 2\pi)$), (iii) three NCNC dimers ($\phi_1 \in [0, \pi)$, $\phi_2 \in [\pi, 2\pi)$), (iv) two triangular trimers ($\phi \in [0, 2\pi)$), (v) two NCNCNC trimers ($\phi \in [0, 2\pi)$). For approach (i), we applied $d_{min} = 9$ Å and $d_{max} = 18$ Å, and in (ii)−(v), we used $d_{min} = 10$ Å and $d_{max} = 20$ Å. Each initial hexamer geometry was optimized for 100 BH steps, corresponding to 100 000 BH steps in total. The three lowest-energy structures from each approach were further optimized for another 100 BH steps using BHPT with 32 replicas. The temperatures of the replicas were exponentially distributed between 270 and 5000 K. The high temperature limit was chosen to facilitate the acceptance of structural changes in the oligomers. It turned out that approaches (iv) and (v), that is, the generation of hexamers from trimers, were most successful, whereas the hexamers produced from monomers had higher energies. However, the structures from approaches (i)−(iii) are very similar to the low-energy structures from (iv) and (v), and would probably reach lower energies upon further optimization. The two most stable hexamers, with $E = -7665.2$ and -7659.8 kcal mol^{-1}, are shown in Figure 4 and are denoted 3NCNCb and 3CNNCb, respectively. Double-layered β-sheets with three peptides per sheet were also observed. The most stable of them are those with two NCNCNC trimers, as shown in Figure 4c. The potential energy of this structure is -7644.1 kcal mol^{-1}, and we identify it as 2NCNCNCb.

3.2.4. Octamers. For the octamers, we generated (i) 200 structures from four CNNC dimers, (ii) 200 structures from four NCNC dimers, (iii) 600 structures from two 2CNNCb tetramers, (iv) 600 structures from two 2NCNCb tetramers, (v) 400

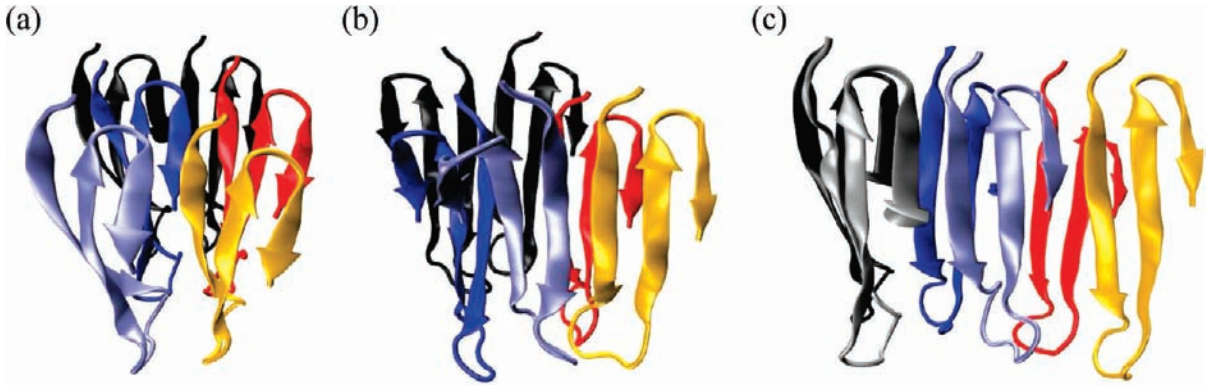

Figure 4. The hydrophobic core-spanning parts of the hexamer structures (a) 3NCNCb, (b) 3CNNCb, and (c) 2NCNCNCb. For each Aβ_{1-42} peptide, only residues 17−42 are illustrated.

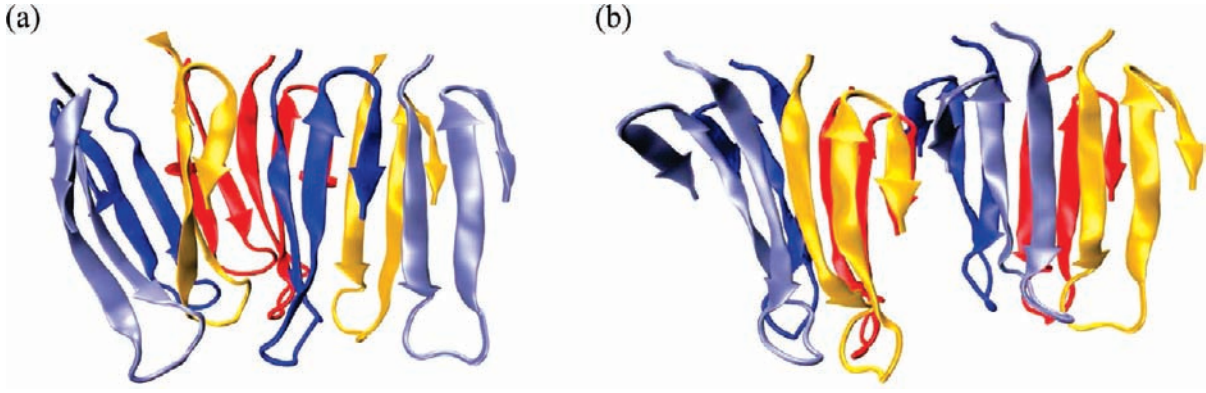

Figure 5. The hydrophobic core-spanning parts of the octamer structures (a) OCTR and (b) OCTS. For each Aβ_{1-42} peptide, only residues 17−42 are illustrated.

structures from two 4NCb tetramers. For approaches (i) and (ii), we used $d_{min} = 10$ Å, $d_{max} = 20$ Å, $\phi_i \in [2(i-1)\pi/3, 2i\pi/3)$ with $i = 1, ..., 3$; for (iii) and (iv), $d_{min} = 20$ Å, $d_{max} = 30$ Å, $\phi \in [0, 2\pi)$; and for approach (v), $d_{min} = 25$ Å, $d_{max} = 40$ Å, $\phi \in [0, 2\pi)$. Each generated structure was optimized for 80 BH steps, corresponding to a total of 160 000 BH steps. The five best structures from each approach were further optimized using BHPT for 80 BH steps and 32 replicas, with temperatures distributed between 270 and 5000 K.

One interesting observation is that the extension of the ordered β-sheets for the hexamers, shown in Figure 4, to octamers does not give the lowest-energy structures. For instance, the extension of 3CNNCb to 4CNNCb leads to a structure with $E = -10\,235$ kcal mol^{-1}. This value is, however, only slightly higher than the energies of the most stable structures shown in Figure 5, which can be characterized as displaced tetrameric units. One of the tetramers is either rotated by about 60−90°, as in Figure 5a, or shifted, as in Figure 5b. These two structures, denoted as OCTR and OCTS, have $E = -10\,243.9$ and $-10\,241.2$ kcal mol^{-1}, respectively. The structure in Figure 5a is composed of two 2NCNCb tetramers. However, stable OCTR structures with energies below $-10\,240$ kcal mol^{-1}, which are composed of one 2NCNCb tetramer and one 2CNNCb tetramer, were observed as well. Octamers with two 2CNNCb units are of the OCTS type, rather than OCTR. In the shifted octamer structure, the stabilization due to interpeptide interactions is clearly smaller compared to OCTR. This difference is compensated by a decrease in ΔG_{solv} due to the larger solvent-accessible surface area in OCTS.

Figure 6. Single-layered octamers form a semicircle in the membrane. Only residues 17−42, which are in the hydrophobic core of the bilayer, are shown for each peptide.

The energy gap between the most stable structures and double- or single-layered β-sheets widens further compared to the hexamer. The most stable double-layered β-sheet, which can be viewed as an extension of the 2NCNCNCb hexamer in Figure 4c, has $E = -10\,212.2$ kcal mol^{-1}, that is, it lies more than 30 kcal mol^{-1} above the most stable octamer. Even higher in energy are the single-layered β-sheets, which form a semicircle in the membrane, as shown in Figure 6, with energies around $-10\,080$ kcal mol^{-1}. The diameter of the full circle consisting of 16 Aβ_{1-42} peptides would be between 7 and 8 nm. From AFM, it was found that Aβ pores in membranes have an inner diameter of about 2 nm and an outer diameter between 8 and 12 nm.[14] For energetic and structural reasons, we can thus exclude the single layered β-sheet barrel as a possible Aβ pore structure. Such a geometry would also not explain the shape of the pores seen in the AFM images, which exhibit rectangular

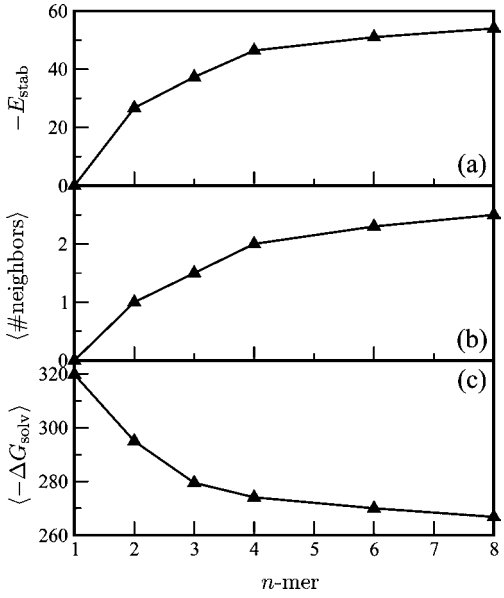

Figure 7. In panel a, the negative stabilization energy per peptide, $-E_{stab}$ (in kcal mol^{-1}), is shown for the most stable membrane-inserted β-sheets composed of n Aβ_{1-42} peptides. In panel b, the average number of direct neighbors, and in panel c, the average negative solvation free energy, $\langle -\Delta G_{solv} \rangle$ (in kcal mol^{-1}), per peptide molecule in these β-sheets are presented.

structures with four subunits and hexagonal structures with six subunits. Furthermore, one would then expect a 16-mer to be the predominant species for the single layered β-sheet barrel, as opposed to tetramers and hexamers, which are actually found from biochemical analysis of the Aβ pores.[11]

3.3. Small β-Sheets as Subunits for Aβ Pores. For the most stable β-sheets presented in the previous section, we have calculated the stabilization energy per peptide as

$$E_{stab} = \frac{E_{n\text{-mer}} - nE_{1\text{-mer}}}{n} \quad (3)$$

where $E_{1\text{-mer}} = -1226.5$ kcal mol^{-1} is the energy of the membrane spanning monomer in Figure 1a and $E_{n\text{-mer}}$ is the energy obtained for the most stable oligomer composed of n Aβ_{1-42} peptides. The results of this analysis in Figure 7a show that the stabilization per peptide increases (i.e., a decrease in E_{stab}) with oligomer size. The stabilization energy seems to reach a limit at $E_{stab} \approx -55$ kcal mol^{-1} for octamers and larger oligomers. The increase in stabilization is due to favorable peptide−peptide interactions, as the average number of direct neighbors per peptide increases with the size of the β-sheet. However, the growth of the average number of direct neighbors decreases from the dimer to the octamer. Each peptide has one neighbor in the dimer, 1.5 neighbors in the triangular trimer, two in the tetramer, and on average 2.5 in the octamer OCTR. The progression of the graphs for $-E_{stab}$, and the average number of neighbors in Figure 7, panels a and b, respectively, is very similar. The opposite trend is seen for the negative solvation free energy averaged over the peptides, $\langle -\Delta G_{solv} \rangle$, which is highest for the monomer and decreases with oligomer size because the monomer is completely surrounded by the solvated membrane, whereas in the oligomers, parts of each peptide are shielded by its neighbors from the solvent and membrane. A higher number of peptide neighbors, thus, leads to a lower solvent-accessible surface area.

The gain in stabilization due to peptide−peptide interactions is larger than the reduction in stabilization due to the diminished peptide-membrane/solvent interactions, leading to an overall growth in $-E_{stab}$ with increasing oligomer size. However, we expect this stabilization to reach a limit for larger β-sheet oligomers, since with increasing n the number of direct neighbors tends to three for ordered β-sheets consisting of 2 or n/2 layers. To increase the number of peptide−peptide contacts, larger ordered β-sheets have to separate into distinct units that are shifted and rotated with respect to each other. This behavior appears to begin for the octamer OCTR and OCTS structures. For larger β-sheets, this effect would eventually lead to a closed geometry forming a channel in the membrane. We thus suggest that the Aβ pores observed in AFM experiments[11−14,24] may consist of tetrameric and hexameric β-sheet subunits such as those we have characterized using the BH approach in Figures 3 and 4. In our model, four to six such subunits would form a pore in the membrane, leading to 16−36 Aβ_{1-42} peptides in the pore. The $C_\alpha - C_\alpha$ distances in the β-sheet tetramers and hexamers show the classic cross-β values of about 4.7 Å between strands in a β-sheet and 10.6 Å between sheets, as is usually observed for amyloid fibrils in X-ray diffraction data.[122] Taking the side chains into account, the tetramers in Figure 3a,b thus have a width of about 2.5−3.0 nm and a depth of 2 nm. The hexamers in Figure 4a,b have the same width but a depth of about 3.5 nm, as illustrated in the Supporting Information. The assembly of four to six such oligomers around a central pore of 2 nm diameter would result in an outer diameter of 8−12 nm.[14] Furthermore, we predict that the tetrameric and hexameric β-sheet subunits are quite stable in a membrane environment, which would explain the occurrence of tetramers and hexamers in the biochemical analysis of Aβ pores.[11] Further studies investigating our Aβ pore model are currently in progress.

In a future study, we will also address the entropic effects on oligomerization. The free energy of association of two molecules may be decomposed into favorable and unfavorable contributions, where the loss of three translational and three (two for linear molecules) rotational degrees of freedom is entropically highly unfavorable. The results in Figure 7 show that this loss of entropy, and the reduced energetic stabilization originating from solvation, can be offset by a favorable binding enthalpy. Furthermore, a significant amount of entropy can be recovered from the six new vibrational degrees of freedom, which correspond to the lost translational and rotational motions, and the altered density of states upon association.[123] From a normal-mode analysis for the dimerization of insulin, a vibrational entropy increase of 24 cal mol^{-1} K^{-1} was calculated.[123] Values differing by one order of magnitude have been reported for the loss of translational entropy during dimerization of macromolecules in solution at standard concentration. If one uses, for instance, the cratic or mixing entropy upon binding,[124] one obtains a value of $-R \ln(1/55) = -8.03$ cal mol^{-1} K^{-1} (R is the ideal gas constant) for the dimerization in a 1 M standard aqueous solution (containing 55 M water). However, in a critical review of the statistical thermodynamic basis for the calculation of binding energies,[125] it was concluded that the cratic entropy is not a useful concept since it lacks a well-defined theoretical

(122) Sunde, M.; Serpell, L. C.; Bartlam, M.; Fraser, P. E.; Pepys, M. B.; Blake, C. C. F. *J. Mol. Biol.* **1997**, *273*, 729–739.
(123) Tidor, B.; Karplus, M. *J. Mol. Biol.* **1994**, *238*, 405–414.
(124) Gurney, R. W. *Ionic Processes in Solution*; McGraw-Hill: New York, 1953.

basis. On the other hand, in experiment,[126] the translational entropy cost of protein association was measured at about 5 cal mol^{-1} K^{-1} which is close to the above value, but about an order of magnitude lower than predicted from other approaches.[123,127] In refs 123, 127, the rotational entropy loss for the insulin dimer was found to be about the same as the translational entropy loss, which is offset by the vibrational entropy gain. Tidorf and Karplus thus find a total entropy loss of 67 cal mol^{-1} K^{-1} for the dimerization of insulin.[123]

In the present study, the β-sheet monomer is roughly linear, leading to a smaller rotational entropy loss upon dimerization and oligomerization. We can estimate lower and upper limits for the entropy change on addition of a monomer to an existing oligomer (or a monomer in the case of dimerization) as follows. The lower limit at a temperature of 300 K derives from refs 124, 126 and is estimated at about 3 kcal mol^{-1} (or even lower), while the upper limit is probably about 15 kcal mol^{-1}.[123,127] The lower limit would not change our results regarding the stability of the observed oligomers up to the octamer very much. The upper limit, on the other hand, would drive the stability in favor of smaller oligomers up to tetramers (compare with Figure 7). Once again, this effect would probably not affect our Aβ pore model significantly, since the structure is predicted to consist of loosely attached tetramers or hexamers. We note that the lower and upper limits given here for the total entropy loss upon Aβ oligomerization in a membrane are only estimates based on previous experiments[126] and theoretical modeling,[123,124,127] in most cases for the insulin dimer in aqueous solution. Further work will be needed to provide quantitative results for Aβ oligomerization.

Our predicted Aβ pore structure is similar to the one proposed by Nussinov and co-workers.[57,58,60,61] Both models predict mobile subunits as basic components of the pore, where the subunits are tetra- to hexamers formed by the Aβ peptides, each exhibiting the typical β-strand-turn-β-strand motif between residues 17−36. The differences between the two models derive from the methodologies employed and the structure of the subunits. While we predict β-sheets as shown in Figures 3 and 4 as the most likely subunit structures, Nussinov and co-workers propose a structure based on the fibril where only parallel β-sheets are formed between the peptides. By means of infrared spectroscopy it was shown, however, that the β-sheets in oligomers are different from the ones in fibrils.[128] The infrared spectra for Aβ_{1-42} oligomers are indicative of β-sheets with parallel and antiparallel arrangements and resemble those of pore-forming porins.[128] The oligomer structure used by Nussinov and co-workers was not observed in our BH simulations, probably because we have focused on the full-length Aβ_{1-42}, while Nussinov et al. investigated the Aβ fragments Aβ_{9-42} and Aβ_{17-42}. The influence of the N-terminal region is therefore missing in the previous model. On the other hand, our model uses an implicit membrane representation to facilitate sampling, neglecting atomistic level Aβ-bilayer interactions. To arrive at an Aβ pore model, we have employed a bottom-up approach starting with the structures predicted to be favorable for the membrane-inserted monomer and small oligomers as possible subunits. Alternatively, Nussinov et al. constructed annular channels guided by NMR data for Aβ fibrils and studied the stability of such channels using MD. The investigation of the whole Aβ channel using our global optimization approach is currently underway.

4. Conclusions

We used basin-hopping (BH) global optimization[62,63] to identify the most stable structures for the Aβ_{1-42} peptide monomer and small oligomers up to the octamer inserted into a lipid bilayer. To improve the efficacy of the BH approach in locating the global potential energy minimum, we employed basin-hopping parallel tempering (BHPT). In this scheme, multiple BH runs of the same system (replicas) are run simultaneously at different temperatures and can be exchanged, provided that the replicas in question are at neighboring temperatures and a Metropolis criterion is satisfied. Another approach that we introduced to initiate each BH run is based on an oligomer generation procedure, which allows us to generate a random oligomer structure from monomers or smaller oligomers. The individual units of the oligomer can be of different types, including different proteins or nonproteinaceous molecules, and are not restricted in terms of their initial conformations. For dimers, our approach allows access to all possible configurations, thus, enabling us to probe the binding modes of protein−protein or protein−ligand complexes.

In the current study, we employed BH for the Aβ_{1-42} monomer and the BHPT approach with initial oligomer generation to investigate Aβ_{1-42} dimers to octamers in the membrane. To represent the effects of the solvent and the membrane, we used the implicit membrane model IMM1,[64] which is implemented in the CHARMM19 force field.[66] The most stable geometry for the monomer in the membrane was identified as a membrane-spanning structure, which is inserted into the hydrophobic membrane core from residue 17 onward and exhibits a typical strand-turn-strand motif between residues 17 and 36,[44,45] with an additional motif of the same sort between residues 35 and 42. On the basis of this structure, we have identified the most stable membrane-inserted oligomers. Analysis of these structures shows that the dimers prefer forming β-sheets in the membrane. The three most stable dimers can be viewed as building blocks for the most favorable structural patterns found in the higher oligomers. The most stable structures obtained for the trimer were β-sheets and equilateral triangular shapes, while for the tetramers and hexamers, β-sheets with two or three layers appear to be preferred. The most stable octamers for the potential function considered here are composed of two tetramers, which are either rotated or shifted with respect to each other. The coordinates of the transmembrane β-sheet monomer is provided in Supporting Information. This structure along with those of the most stable oligomers are also available from the Cambridge Cluster Database.[129]

The stabilization per peptide in an oligomer compared to the membrane-spanning monomer increases with oligomer size and reaches a limit for octamers and larger oligomers. Favorable peptide−peptide interactions, resulting from the increase in the average number of nearest-neighbors per peptide with increasing β-sheet size, lead to this gain in stabilization. This effect outweighs the loss of peptide-membrane/solvent interactions. However, since the average number of nearest-neighbors per

(125) Gilson, M. K.; Given, J. A.; Bush, B. L.; McCammon, J. A. *Biophys. J.* **1997**, *72*, 1047–1069.
(126) Tamura, A.; Privalov, P. L. *J. Mol. Biol.* **1997**, *273*, 1048–1060.
(127) Finkelstein, A. V.; Janin, J. *Protein Eng.* **1989**, *3*, 1–3.
(128) Cerf, E.; Sarroukh, R.; Tamamizu-Kato, S.; Breydo, L.; Derclaye, S.; Raussens, V. *Biochem. J.* **2009**, *421*, 415–423.
(129) Wales, D. J.; Doye, J. P. K.; Dullweber, A.; Hodges, M. P.; Naumkin, F. Y.; Calvo, F.; Hernández-Rojas, J.; Middleton, T. F. The Cambridge Cluster Database, URL http://www-wales.ch.cam.ac.uk/CCD.html, 2001.

peptide tends to three for ordered β-sheets, we expect the stabilization to reach a limit for larger oligomers. This limit causes larger β-sheets to separate into smaller distinct units, which are shifted and rotated with respect to each other, in order to increase the number of peptide−peptide contacts. The most stable octamer structures identified in the current study already exhibit this effect. We thus suggest that the Aβ pores observed in AFM experiments[11−14,24] may consist of tetrameric and hexameric β-sheet subunits corresponding to structures similar to the ones we have characterized in the present work. This Aβ pore model is in accord with the size and shape considerations from AFM experiments[14] and biochemical analysis.[11]

Acknowledgment. B.S. gratefully acknowledges the Jülich Supercomputing Centre for providing and maintaining the computing resources used in this work. C.S.W. thanks the EPSRC for financial support.

Supporting Information Available: Sample input for a basin-hopping run with the GMIN program together with annotations, additional figures for the most stable tetramers and hexamers, coordinates for the transmembrane β-sheet monomer, and complete refs 93 and 104. This material is available free of charge via the Internet at http://pubs.acs.org.

JA103725C